MNRAS 000, 1–13 (2015) Preprint 16 November 2016 Compiled using MNRAS LATEX style file v3.0

Environmental impacts on dust temperature of star-forming galaxies in the local Universe

Yasuhiro Matsuki[1,2⋆], Yusei Koyama[3,4], Takao Nakagawa[1] and Satoshi Takita[1]
[1] *Institute of Space Astronautical Science, Japan Aerospace Exploration Agency, Sagamihara, Kanagawa 252-5210, Japan*
[2] *Department of Physics, Graduate School of Science, The University of Tokyo, Tokyo 113-0033, Japan*
[3] *Subaru Telescope, National Astronomical Observatory of Japan, National Institutes of Natural Sciences, 650 North A'ohoku Place, Hilo, HI 96720, USA*
[4] *Graduate University for Advanced Studies (SOKENDAI), Osawa 2-21-1, Mitaka, Tokyo 181-8588, Japan*

arXiv:1611.04609v1 [astro-ph.GA] 14 Nov 2016

Accepted XXX. Received YYY; in original form ZZZ

ABSTRACT

We present infrared views of the environmental effects on the dust properties in star-forming (SF) galaxies at $z \sim 0$, using the AKARI Far-Infrared Surveyor (FIS) all-sky map and the large spectroscopic galaxy sample from Sloan Digital Sky Survey (SDSS) Data Release 7 (DR7). We restrict the sample to those within the redshift range of $0.05 < z < 0.07$ and the stellar mass range of $9.2 < \log_{10}(M_*/M_\odot)$. We select SF galaxies based on their Hα equivalent width ($EW_{\mathrm{H}\alpha} > 4$ Å) and emission line flux ratios. We perform far-infrared (FIR) stacking analyses by splitting the SDSS SF galaxy sample according to their stellar mass, specific SFR ($SSFR_{\mathrm{SDSS}}$), and environment. We derive total infrared luminosity (L_{IR}) for each subsample using the average flux densities at WIDE-S (90 μm) and WIDE-L (140 μm) bands, and then compute IR-based SFR (SFR_{IR}) from L_{IR}. We find a mild decrease of IR-based $SSFR$ ($SSFR_{\mathrm{IR}}$) amongst SF galaxies with increasing local density ($\sim$ 0.1-dex level at maximum), which suggests that environmental effects do not instantly shut down the SF activity in galaxies. We also derive average dust temperature (T_{dust}) using the flux densities at 90 μm and 140 μm bands. We confirm a strong positive correlation between T_{dust} and $SSFR_{\mathrm{IR}}$, consistent with recent studies. The most important finding of this study is that we find a marginal trend that T_{dust} increases with increasing environmental galaxy density. Although the environmental trend is much milder than the $SSFR$–T_{dust} correlation, our results suggest that the environmental density may affect the dust temperature in SF galaxies, and that the physical mechanism which is responsible for this phenomenon is not necessarily specific to cluster environments because the environmental dependence of T_{dust} holds down to relatively low-density environments.

Key words: galaxies: star formation – ISM: dust.

1 INTRODUCTION

It is widely known that various galaxy properties, such as star formation rate (SFR) or morphologies, strongly depend on the local galaxy environment (Blanton & Moustakas 2009). In the local Universe, Dressler (1980) investigated 55 rich clusters and found that the fraction of elliptical galaxies increases with local galaxy density, while that of spiral galaxies decreases towards high-density regions. Goto et al. (2003) showed similar results based on the Sloan Digital Sky Survey (SDSS) Early Data Release. Balogh et al. (1997) found that the average SFR for cluster galaxies is lower than the average for field galaxies. Lewis et al. (2002) and Gómez et al. (2003) also showed that SFR decreases with increasing local galaxy density.

For star-forming (SF) galaxies, it is established that SFR increases with stellar mass (M_*). This SFR–M_* relation for SF galaxies is often called the "SF main sequence", and recognized both in the local Universe (Brinchmann et al. 2004; Peng et al. 2010) and in the distant Universe (Daddi et al. 2007; Noeske et al. 2007; Whitaker et al. 2012). Peng et al. (2010) studied local SF galaxies using SDSS seventh Data Release (DR7) and found that the SFR–M_* relation is independent of the environment. Wijesinghe et al. (2012) showed a similar result by using galaxies observed in the Galaxy And Mass Assembly (GAMA), and concluded that the SFR–density relation is largely driven by the higher fraction of passive early-type galaxies in high-density environ-

⋆ E-mail: matsuki@ir.isas.jaxa.jp

© 2015 The Authors

ments. The environmental independence of the SF main sequence is also suggested for high-redshift galaxies out to $z \sim 2$ (Koyama et al. 2013). These results claiming small (or lack of) environmental dependence of the SF main sequence may suggest a rapid SF quenching mechanism at work in high-density environments.

However, environmental variations in the properties of star-forming galaxies is still under debate. Some recent studies showed small, but significant environmental dependence of SF activity amongst SF galaxies. Haines et al. (2013) found that specific SFR ($SSFR$) of SF cluster galaxies is lower than that of SF galaxies in field environments by using a sample of 30 massive galaxy clusters at $0.15 < z < 0.30$ from the Local Cluster Substructure Survey (LoCuSS). Similarly, by using the data from Herschel Astrophysical Terahertz Large Area Survey (H-ATLAS), Fuller et al. (2016) showed that $SSFR$ of late-type galaxies in the Coma cluster declines with increasing their local galaxy number density. In $0.6 < z < 0.8$, Vulcani et al. (2010) found the $SSFR$ reduction of star-forming galaxies of the same mass in cluster environments by using 24 μm MIPS/Spitzer data. Fuller et al. (2016) also found that gas-to-stars ratio decreases with increasing environmental density. These results can be explained if the gas content of galaxies is stripped when they enter cluster environments.

The gas removal (or reduction) of galaxies is one of the main causes for SF quenching in galaxies. Although the dominant mechanism responsible for quenching is still under debate, many possible physical mechanisms are proposed as the driver of environmental effects: e.g. ram-pressure stripping of the cold gas due to interaction with the intracluster medium (Gunn & Gott 1972; Quilis et al. 2000), galaxy harassment through high velocity encounters with other galaxies (Moore et al. 1999), suppression of the accretion of cold gas: *strangulation* (Feldmann et al. 2011; Bekki 2009; Kawata & Mulchaey 2008; Larson et al. 1980), and galaxy mergers or close tidal encounters of galaxies in in-falling groups (Zabludoff & Mulchaey 1998).

Understanding the dust properties in galaxies is very important when we discuss SF activity in galaxies because dust absorbs a large fraction of the UV light emitted by O/B-type stars and reradiates it in far-infrared (FIR). The Hα emission, which is often used as a good indicator of SFR, can also be significantly attenuated by interstellar dust grains in the case of extremely dusty galaxies (Poggianti & Wu 2000; Koyama et al. 2010). FIR observations are thus crucial to study SF activity hidden by dust. In particular, the dust temperature ($T_{\rm dust}$) can be an important factor because $T_{\rm dust}$ is expected to be linked to the physical conditions prevailing in the SF regions within galaxies. In fact, it is suggested that galaxies with higher $SSFR$ tend to have higher dust temperature due to the strong ultraviolet (UV) radiation fields of the young massive stars (Magnelli et al. 2014).

It is shown that the distribution of dust component within galaxies well traces that of molecular gas contents (Cortese et al. 2012). Also, dust temperatures are typically higher in the central part of galaxies than in the outskirts (Engelbracht et al. 2010). It is expected that stripping effects tend to remove gas and dust from outskirts of galaxies (Diemand et al. 2007). If molecular gas of galaxies is really stripped in high-density regions, cold dust in the outskirts of SF galaxies could also be stripped, which could result in warm dusts in the inner parts of galaxies being exposed. Therefore, we expect that dust temperatures of SF galaxies increase with their local densities.

A few recent studies actually claim a correlation between $T_{\rm dust}$ and environments. Rawle et al. (2012) studied $z \sim 0.3$ galaxy clusters with *Herschel*, and found that *warm dust* galaxies are preferentially located in cluster environments. They attribute this result to *cold* dust stripping effects at work in cluster environments. In contrast, Noble et al. (2015) showed that $T_{\rm dust}$ tends to be lower in the cluster environments at $z \sim 1$. They interpreted this as a result of *warm* dust stripping effects. There is no systematic study on the environmental effects on dust temperatures in galaxies so far. This is primarily because dust temperature measurements require multi-band photometry at FIR, and that huge area survey at FIR is required if we really want to perform studies on environmental effects on dust temperatures of galaxies in an unbiased way.

In this paper, we study environmental effects on *hidden* SF activities in galaxies, particularly focusing on IR-based $SSFR$ and dust temperatures, by using the newly released AKARI FIR all-sky survey map and SDSS DR7 spectroscopic sample. Because of the limited depths of FIR all-sky survey performed by AKARI, we will focus on the average properties of galaxies by exploiting FIR stacking analyses.

This paper is organized as follows. In Section 2, we describe the outline of our sample selection, local density measurements, as well as the technique of our stacking analyses. In Section 3, we present the dependence of $SSFR$ on local density. The main result of this study is presented in Section 4, where we study the environmental dependence of average dust temperature of galaxies in the local Universe. Because it is expected that dust temperature is strongly correlated with $SSFR$ (Magnelli et al. 2014), we also examine the environmental dependence of $T_{\rm dust}$ at fixed $SSFR$. We compare our results with some recent studies and discuss possible explanations for the dependence of $T_{\rm dust}$ on local density. In Section 5, we summarize our conclusions.

Throughout the paper, we adopt $\Omega_{\rm M} = 0.3$, $\Omega_{\Lambda} = 0.7$ and $H_0 = 70\ {\rm km\,s^{-1}\,Mpc^{-1}}$. We assume Kroupa (2001) initial mass function (IMF) to derive physical quantities in order to keep consistency with those derived in the literatures.

2 DATA

2.1 Sloan Digital Sky Survey

2.1.1 Definition of environment

In this work, we define the galaxy environment by computing the local density of galaxies. We here describe the outline of our density measurements.

We use the SDSS (DR7; Abazajian et al. 2009) spectroscopic data. Some galaxy properties (e.g. redshift or stellar mass) are derived by Max Planck Institute for Astropysics and Johns Hopkins University group (MPA/JHU group). We retrieve their "value-added" catalogue (hereafter MPA/JHU catalogue) from their website[1]. The catalogue contains a

[1] http://wwwmpa.mpa-garching.mpg.de/SDSS/DR7

magnitude limited sample of 927,552 galaxies (with Petrosian 1976 magnitude limit of $r' \leq 17.77$).

SDSS covers a contiguous area of ~ 7500 deg^2 in Northern Galactic Cap and the three stripes in the Southern Galactic Cap. We select a sample of 771,693 galaxies within the area of $105° <$ R.A. $< 270°$ and $-5° <$ DEC. $< 75°$, corresponding to the contiguous region, which is better suited for environmental studies. Then, we exclude duplicated objects by performing internal matching with maximum separation of 1″, yielding 738,143 objects as unique sources.

We calculate the local density of each galaxy using projected n-th nearest neighbour surface density Σ_n, which is expressed as

$$\Sigma_n = \frac{n}{\pi {D_{p,n}}^2} \quad (\mathrm{Mpc}^{-2}), \tag{1}$$

where $D_{p,n}$ is the projected comoving distance to the n-th nearest neighbour within a velocity window of ± 1000 km s^{-1}, or equivalently a redshift slice of $\Delta z = \pm 0.003$. Note that the size of this velocity window (± 1000 km s^{-1}) corresponds to a typical velocity dispersion of galaxy clusters, and so we believe that it is wide enough to pick out the physically related galaxies.

Because the original sample is magnitude limited, we need to take into account the redshift dependence of the completeness limits. We therefore define the normalized local galaxy number density (ρ_n) as follows:

$$\rho_n = \frac{\Sigma_n}{\langle \Sigma_n \rangle}, \tag{2}$$

where $\langle \Sigma_n \rangle$ is the median Σ_n of galaxies at each redshift within a slice of $\Delta z = \pm 0.003$. In this paper, we fix to $n = 5$.

2.1.2 *Selection of star-forming galaxies*

In this section, we describe the outline of our sample selection. Our procedure is also summarized in Fig. 1.

We first restrict the sample to galaxies within the redshift range of $0.05 < z < 0.07$. We exclude very low-z galaxies (at $z < 0.05$) because the limited size of SDSS fibre (3 arcsec) covers only a fraction of their total lights. Kewley et al. (2005) suggest that at least $> 20\%$ of galaxy light should be covered by the fibre to reduce systematic errors from aperture effects. According to Kewley et al. (2005), $z > 0.04$ is required in the case of SDSS to ensure a covering fraction of $> 20\%$ for a typical galaxy. We note that we also apply a relatively narrow redshift range so that we can capture the same rest-frame wavelength range when we perform FIR stacking analyses (see Section 2.2).

We then apply a stellar mass cut of $9.2 < \log_{10}(M_*/M_\odot)$, considering the completeness limit of the SDSS spectroscopic survey (see Fig. 2). Because the SDSS is magnitude limited, it is clear that the stellar mass limit depends on the redshift.

The main aim of this study is to investigate the environmental dependence of star-forming galaxy properties. We select SF galaxies by applying the $EW_{\mathrm{H}\alpha} > 4$ Å and S/N(Hα)> 3 to exclude quiescent galaxies. Then, we use Baldwin, Phillips & Telervich (BPT) diagram, which compares the $F_{[\mathrm{OIII}]5007}/F_{\mathrm{H}\beta}$ and $F_{[\mathrm{NII}]6584}/F_{\mathrm{H}\alpha}$ line flux ratio, to distinguish between star-forming galaxies and active galactic nuclei (Baldwin et al. 1981) (see Fig. 3). For this purpose, we also require S/N > 3 in all the four major lines. Our final sample includes 34,249 SF galaxies to all of which local density measurements are available.

Table 1. The numbers of SDSS star-forming galaxy samples at $0.05 < z < 0.07$ in each environmental bin.

Local Density Bin	Number of Samples
D1	4767
D2	8007
D3	9628
D4	7078
D5	4769

We define the five local density bins as follows:

$$\begin{aligned}
\mathrm{D1} &: \log_{10}\rho_5 \leq -0.55 \\
\mathrm{D2} &: -0.55 < \log_{10}\rho_5 \leq -0.22 \\
\mathrm{D3} &: -0.22 < \log_{10}\rho_5 \leq 0.08 \\
\mathrm{D4} &: 0.08 < \log_{10}\rho_5 \leq 0.36 \\
\mathrm{D5} &: 0.36 < \log_{10}\rho_5
\end{aligned}$$

The size of each density bin is set to ~ 0.3 dex for D2, D3, and D4, while D1 and D5 cover all remaining samples in lower and higher density regions, respectively (see the distribution of $\log_{10}\rho_5$ in the left panel of Fig. 4). The numbers of galaxy samples in each density bin are shown in Table 1.

In Fig. 4 (right), we show the spatial distribution of our SF galaxy samples on the sky. The redder colours indicate galaxies in higher-density environments. For example, D5 galaxies (shown with red dots) tend to be strongly clustered and align filamentary structures, while the D1 galaxies (purple dots) tend to be more widely scattered around. This result further supports the robustness of our local density measurements. We also show in Fig. 5 the fraction of SF galaxies as a function of ρ_5. This plot shows a monotonical decrease of SF galaxy fraction towards higher ρ_5, further supporting the validity of our density measurements.

2.1.3 *Stellar mass and star formation rate*

We use the stellar mass (M_*) estimates from the MPA/JHU catalogue (Kauffmann et al. 2003a; Salim et al. 2007). They are based on fits to the broad-band *ugriz* photometry of the SDSS with Bayesian methodology following the philosophy of Kauffmann et al. (2003a) and Salim et al. (2007). The *ugriz* broad-band magnitudes are corrected for emission lines by assuming that the relative contribution of emission lines to the broad-band magnitudes is the same for inside and outside the fibre, although the effect of emission lines on broad-band magnitudes is reported to be negligibly small (typically < 0.1 magnitude[2]).

We also use Hα-based SFRs calculated for the SDSS DR7 data by the MPA/JHU group (hereafter SFR_{SDSS}). The calculation is based on the technique discussed in Brinchmann et al. (2004), by fitting nebular emission-line fluxes. The fits to star forming galaxies were performed using the

[2] http://wwwmpa.mpa-garching.mpg.de/SDSS/DR7/mass_comp.html

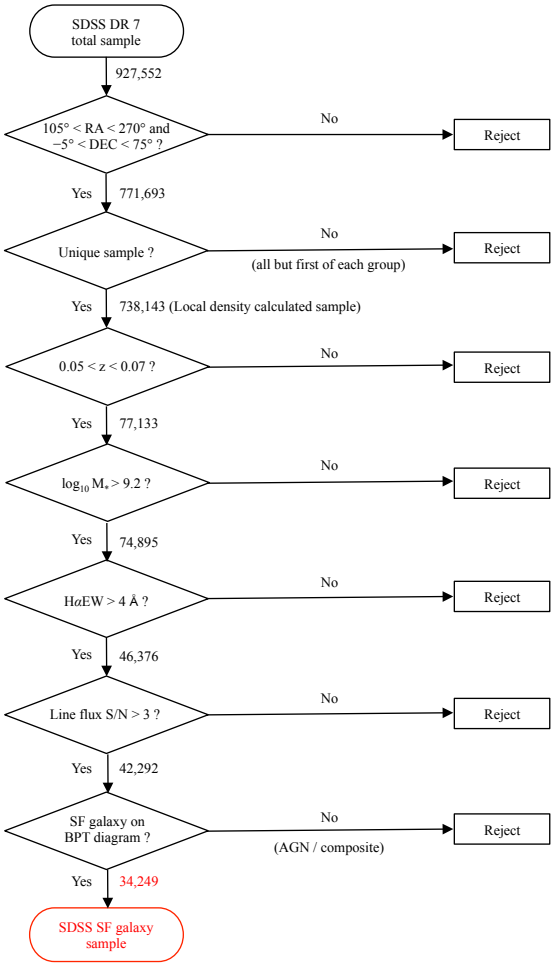

Figure 1. Summary of our sample selection procedure.

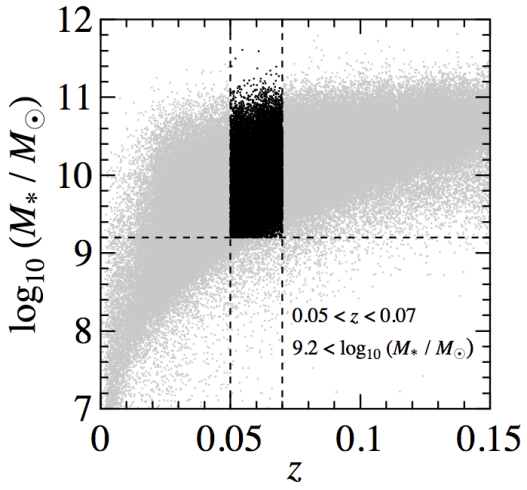

Figure 2. Stellar mass plotted against redshift for all SDSS star-forming galaxies (grey dots). The black dots show the galaxies that we used in this paper.

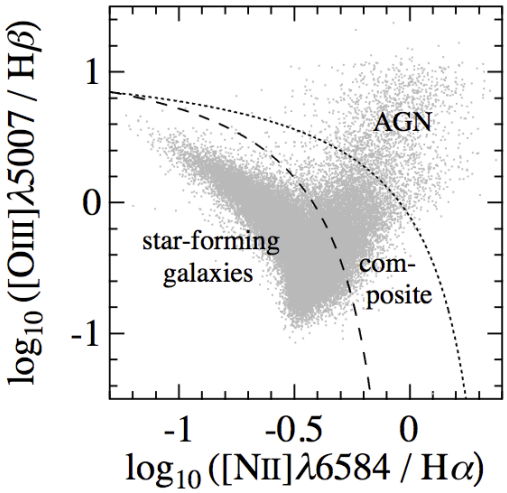

Figure 3. The Baldwin, Phillips & Telervich (BPT) diagram for the 42,292 SDSS galaxies with $EW_{\mathrm{H}\alpha} > 4$ Å and line flux S/N > 3 in $0.05 < z < 0.07$. The dotted and dashed lines are derived from Kewley et al. (2001) and Kauffmann et al. (2003b), respectively.

Charlot & Longhetti (2001) model. To compute the line and continuum emission from galaxies consistently, the model combines population synthesis and photoionization codes. The model assumes that no ionizing radiation escapes the galaxies. The aperture correction was performed following the philosophy of Salim et al. (2007). The dust extinction correction was also done by using the $F_{\mathrm{H}\alpha}/F_{\mathrm{H}\beta}$ line flux ratio.

2.2 AKARI

2.2.1 AKARI all-sky survey map

We here describe the summary of AKARI all-sky survey data. To investigate the environmental dependence of SFR_{IR} and dust temperature (T_{dust}), we use the newly-released AKARI FIR all-sky survey maps by the Far-infrared Surveyor (FIS) (Kawada et al. 2007) on the AKARI satellite (Murakami et al. 2007). The data taken by FIS were pre-processed using the AKARI FIS pipeline tool (Yamamura et al. 2009). The calibrations include corrections for non-linearity and sensitivity drifts of detectors, rejection of anomalous data due to high-energy particles (glitches), signal saturation, and other instrumental effects as well as dark-current subtraction (Doi et al. 2015). After these calibrations, the final FIS image has a pixel scale of 15″ and units of surface brightness in MJy sr^{-1}. The image data are disclosed in FITS format files, and distributed as a number of 6.0×6.0 deg^2 images with ecliptic coordinate[3].

All-sky survey was performed by AKARI in six bands centred at 9, 18, 65, 90, 140 and 160 μm. FIS observed the four longer wavelength bands: i.e. N60, WIDE-S, WIDE-L, and N160, centred at 65, 90, 140, and 160 μm, respectively. The point source flux detection limits (for S/N>5) for one scan are 2.4, 0.55, 1.4 and 6.3 Jy for N60, WIDE-S, WIDE-L and N160, respectively (Kawada et al. 2007). The FIS all-

[3] http://www.ir.isas.jaxa.jp/AKARI/Archive/Images/FISMAP/

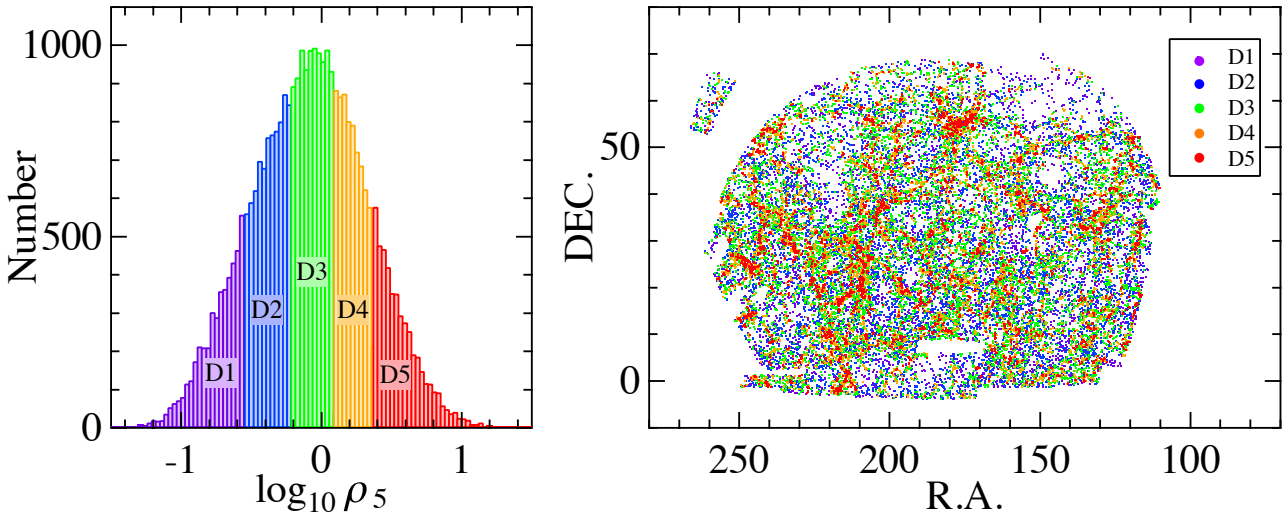

Figure 4. (Left): The distribution of the local galaxy density (ρ_5) for all our SDSS star-forming galaxies. The histogram is created with the bin width of 0.05 dex. (Right): Spatial distribution of our SDSS star-forming galaxy sample on the sky. Redder symbols indicate galaxies in higher-density environments. This plot visually demonstrates the robustness of our density measurements.

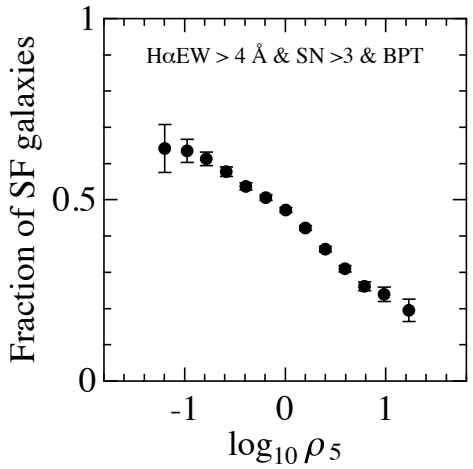

Figure 5. Star-forming galaxy fraction as a function of the local density, showing the monotonical decrease towards high-density environment (as expected). This plot further demonstrates the validity of our density measurements.

sky map covers ~98% of the whole sky, including the SDSS DR7 survey region.

Because of the limited depths of the all-sky survey, we cannot detect the infrared emission from individual galaxies except for very bright sources. We therefore decided to perform stacking analysis to study average properties of SF galaxies (see below).

2.2.2 Stacking analysis

In this section, we describe the procedure of our stacking analysis. We first split the samples into some groups according to their local density (ρ_5), stellar mass, SFR, and $SSFR$. For each galaxy, we retrieve a 6.0×6.0 deg^2 map whose central position is nearest to the target galaxy, and create $20' \times 20'$ cut out image centred at the position of each target galaxy. We note that we fix the y-axis directions of each cut-out image to the FIS scan direction.

Before stacking, we apply the following criteria to discard images which are not suited for the stacking analysis:

(i) Discard the images if the $20' \times 20'$ cutout images protrude from the original 6.0 × 6.0 deg^2 map; i.e. sources located very close to the edge of 6.0×6.0 deg^2 map.
(ii) Discard the images having areas whose $N_{\rm scan}$ value (the number of visit) is 0 or 1 (times) because the pixel values of these regions are very noisy.
(iii) Discard the images that include more than 10 pixels whose values are smaller than -8 MJy sr^{-1}. This problem seems to happen when high-energy particles hit the detector.
(iv) Discard the images having a 3 × 3 region whose total value is unrealistically high (with >300 MJy sr^{-1} for N160 or 200 MJy sr^{-1} for the others bands) at >30″ away from the image centre. This is most likely due to contamination of nearby bright sources.

After applying these criteria, the numbers of frames are decreased by $\lesssim 10\%$, and all the remaining sample are used for stacking. In order to derive their average flux densities of SDSS SF galaxies split according to stellar mass, $(S)SFR$, and environment, we perform average stacking for each subsample. We show in Fig. 6 how the noise levels can be reduced by stacking 1, 10, 100, 1,000, and 10,000 frames at the positions of galaxies with $9.2 < \log_{10} M_* < 9.8$ (for WIDE-S band data). This demonstrates that we can measure the average FIR fluxes of faint low-mass galaxies by adopting stacking analysis. Fig. 7 shows this result more quantitatively; the noise level is reduced following $\propto N_{\rm stack}^{-1/2}$ (as expected) for both WIDE-S and WIDE-L data.

We perform aperture photometry on the final stacked images. It is suggested that there is no systematic correlation between the source flux densities and the PSFs (Arimatsu et al. 2014), and so we assume that all sources have the

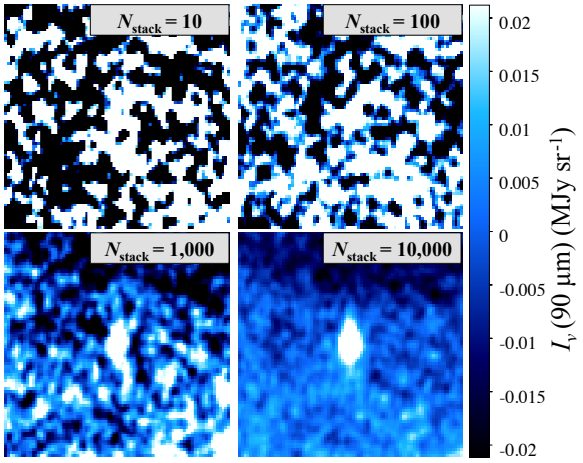

Figure 6. Examples of the WIDE-S "stacked" images for galaxies with $9.2 < \log_{10} M_* < 9.8$, demonstrating the increase of signal-to-noise ratio by coadding a number of frames. The size of each image is $20' \times 20'$. The numbers of coadded frames ($N_{\rm stack}$) are indicated in each panel. The colour bar shows the scale of the intensities (I_ν) at 90 μm.

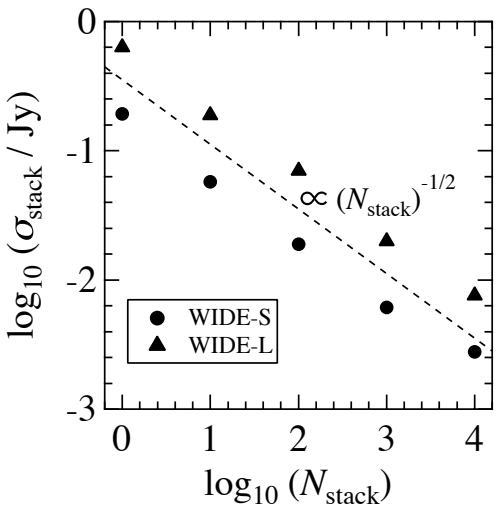

Figure 7. The random noise levels for the stacked images for WIDE-S and WIDE-L bands as a function of the number of coadded frames ($N_{\rm stack}$). This plot demonstrates that the noise levels can be reduced with $\propto N_{\rm stack}^{-1/2}$ (see texts for details how we determine the noise levels of the stacked images).

same PSF at each band. The full width at half maximum (FWHM) of PSFs are 63.4 ± 0.2, $77.8 \pm 0.2''$ and $88.3 \pm 0.9''$ at N60, WIDE-S and WIDE-L bands, respectively, hence we can assume that our target galaxies at $0.05 < z < 0.07$ are point sources. Note that the PSF at the N160 band is not determined because of the limited number of bright standard stars for this band (Takita et al. 2015). The shape of the PSF at each band is anisotropic, especially for WIDE-S band, but we adopt simple circular aperture photometry with a reasonably large aperture size. We set an aperture radius to $90''$ and a sky background annulus area to 120–$300''$ radius, to be consistent with the procedure shown by Takita et al. (2015).

We follow the flux calibration for each band as shown by Takita et al. (2015). The mean observed-to-expected flux density ratios in the case of the above aperture photometry parameters are 0.627 ± 0.029, 0.696 ± 0.008 and 0.381 ± 0.043 for the N60, WIDE-S, and WIDE-L bands, respectively. The calibration for N160 (160 μm) has not yet been done because of the limited number of bright standard stars detected at N160. For this reason, we do not use the 160 μm band when we derive $SFR_{\rm IR}$ and $T_{\rm dust}$. In addition, it is suggested that the stochastic heating of very small grains affects the 65 μm fluxes of galaxy SEDs (Draine 2003; Compiègne et al. 2010). Therefore, we decide to compute $SFR_{\rm IR}$ and $T_{\rm dust}$ analytically by using the 90 μm and 140 μm fluxes.

Assuming that the flux uncertainties are dominated by random background noise (as demonstrated by our analyses in Fig. 7), we determine the flux errors with the following procedure. We first select $N_{\rm stack}$ random positions on the FIS map, and stack them. We then perform aperture photometry on this stacked image in the same way as above. We repeat this process 200 times, and we take the standard deviation of 200 flux densities as our 1σ flux uncertainties. We note that the uncertainties for $SFR_{\rm IR}$ and $T_{\rm dust}$ presented in this work simply reflect the photometric errors estimated here.

3 SPECIFIC STAR FORMATION RATE VERSUS ENVIRONMENT

3.1 Deriving total infrared luminosities ($L_{\rm IR}$)

Interstellar dust absorbs and scatters the UV light from O/B-type stars and re-emit it in far infrared (FIR). Therefore, the total infrared luminosities ($L_{\rm IR}$) are known to be a good tracer for dust-enshrouded star formation activities (Kennicutt 1998; Chary & Elbaz 2001).

In this section, we summarize the method for deriving $SFR_{\rm IR}$. Firstly, we derive $L_{\rm IR}$ by using the AKARI FIR photometry at WIDE-S and WIDE-L bands. Following Takeuchi et al. (2010), we here define $L_{\rm AKARI}^{\rm 2bands}$ as the following:

$$L_{\rm AKARI}^{\rm 2bands} = \Delta\nu_{90\mu{\rm m}} L_\nu(90\mu{\rm m}) + \Delta\nu_{140\mu{\rm m}} L_\nu(140\mu{\rm m}), \quad (3)$$

where $L_\nu(90\mu{\rm m})$ and $L_\nu(140\mu{\rm m})$ are the luminosity densities at WIDE-S and WIDE-L respectively, and

$$\Delta\nu_{90\mu{\rm m}} = 1.47 \times 10^{12}({\rm Hz}) \quad (4)$$

$$\Delta\nu_{140\mu{\rm m}} = 0.831 \times 10^{12}({\rm Hz}) \quad (5)$$

are the band widths for WIDE-S and WIDE-L, respectively (Hirashita et al. 2008). We derive $L_\nu(90\mu{\rm m})$ and $L_\nu(140\mu{\rm m})$ as follows:

$$L_\nu(90\mu{\rm m}) = 4\pi d_{\rm L}^2 \frac{F_\nu(90\mu{\rm m})}{1+z}, \quad (6)$$

$$L_\nu(140\mu{\rm m}) = 4\pi d_{\rm L}^2 \frac{F_\nu(140\mu{\rm m})}{1+z}, \quad (7)$$

where $F_\nu(90\mu{\rm m})$ and $F_\nu(140\mu{\rm m})$ are the observed flux densities at WIDE-S and WIDE-L bands, respectively, and $d_{\rm L}$ is the luminosity distance to each galaxy. Then, $L_{\rm IR}$ is derived from $L_{\rm AKARI}^{\rm 2bands}$ with the following equation shown by Takeuchi et al. (2010):

$$\log_{10}(L_{\rm IR}/L_\odot) = 0.964 \log_{10} L_{\rm AKARI}^{\rm 2bands} + 0.814. \quad (8)$$

To keep consistency with measurements for SDSS Hα-based

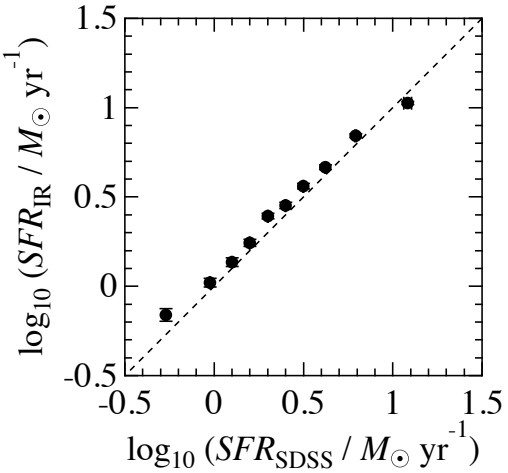

Figure 8. Comparison between the IR-based SFRs ($SFR_{\rm IR}$) and the Hα-based SFRs ($SFR_{\rm SDSS}$) for SDSS star-forming galaxy samples divided into 10 $SFR_{\rm SDSS}$ bins. The dashed line corresponds to: $SFR_{\rm IR}$=$SFR_{\rm SDSS}$. This plot demonstrates that the two independent measurements agree with each other very well.

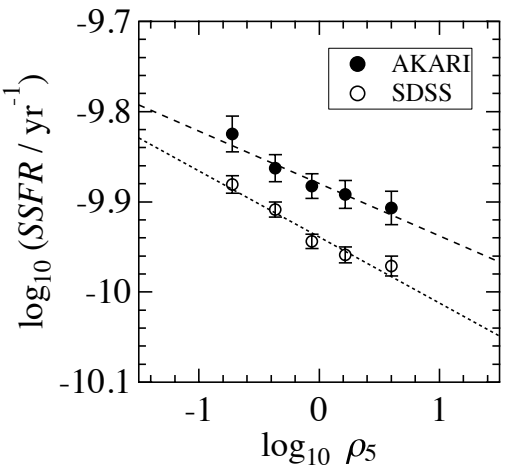

Figure 9. Dependence of the $SSFR_{\rm IR}$ (filled circles) and $SSFR_{\rm SDSS}$ (open circles) on the local density. The dashed and dotted lines are the best fitted lines corresponding to: $\log_{10} SSFR_{\rm IR} = -(9.880 \pm 0.007) - (0.06 \pm 0.02) \times \log_{10}\rho_5$ and $\log_{10} SSFR_{\rm SDSS} = -(9.939 \pm 0.004) - (0.07 \pm 0.01) \times \log_{10}\rho_5$, respectively. We note that the results shown in this diagram are for star-forming galaxies only.

SFRs ($SFR_{\rm SDSS}$), we derive IR-based SFR with the relation from Kennicutt (1998) assuming Kroupa IMF:

$$SFR_{\rm IR}\ (M_\odot\,{\rm yr}^{-1}) = 3.1 \times 10^{-44} L_{\rm IR}\ ({\rm erg\,s}^{-1}). \quad (9)$$

Here we do not take into account the effect of k-correction because the WIDE-S and WIDE-L bands are wide enough, and the effects can be negligible when measuring $L_{\rm IR}$ in the redshift range we are considering. Indeed, it is demonstrated that $SFR_{\rm IR}$s derived with this method show good agreement with SFRs derived from dust-corrected Hα luminosities for $z < 0.1$ galaxies (Koyama et al. 2015). As a further check, we also plot in Fig. 8 our data points (from stacking) on the $SFR_{\rm IR}$–$SFR_{\rm SDSS}$ plane. We here further divide our SF galaxy sample into 10 $SFR_{\rm SDSS}$ bins, and perform the stacking analyses for each subsample to derive their $SFR_{\rm IR}$. It is found that $SFR_{\rm IR}$ are in good agreement with $SFR_{\rm SDSS}$ over wide luminosity range. This result supports the validity of our procedure for deriving $L_{\rm IR}$.

3.2 Environmental dependence of $SSFR$ for SF galaxies

Our primary goal is to investigate the environmental dependence of $T_{\rm dust}$. As shown by Magnelli et al. (2014), there exists a strong correlation between $T_{\rm dust}$ and $SSFR$. Therefore, we must distinguish the effects of environment and $SSFR$. For this purpose, we examine the environmental dependence of IR-based $SSFR$ ($SSFR_{\rm IR}$).

The unit of $SSFR$ is inverse of time, and so $SSFR$ indicates the time-scale of star formation. We calculate both IR- and Hα-based $SSFR$ (hereafter $SSFR_{\rm IR}$ and $SSFR_{\rm SDSS}$). In order to perform fair comparison between $SSFR_{\rm IR}$ (from stacking) and $SSFR_{\rm SDSS}$, we derive the mean $SSFR_{\rm SDSS}$ by dividing the mean SFR by the mean M_* rather than simply averaging the SFR/M_* of individual galaxies: i.e.

$$\langle SSFR\rangle = \frac{\langle SFR\rangle}{\langle M_*\rangle} \neq \left\langle \frac{SFR}{M_*} \right\rangle \quad (10)$$

In Fig. 9, we show the average $SSFR_{\rm IR}$ and $SSFR_{\rm SDSS}$ derived for each local density bin. The best fitted lines to the data points are:

$$\log_{10}(SSFR_{\rm IR}/yr^{-1}) = -(9.880 \pm 0.007) - (0.06 \pm 0.02) \times \log_{10}\rho_5, \quad (11)$$

and

$$\log_{10}(SSFR_{\rm SDSS}/yr^{-1}) = -(9.939 \pm 0.004) - (0.07 \pm 0.01) \times \log_{10}\rho_5. \quad (12)$$

The best fitted lines show negative slope, indicating that both $SSFR_{\rm IR}$ and $SSFR_{\rm SDSS}$ monotonically decrease with increasing ρ_5. We note that our sample includes *only SF galaxies*. Recent studies reported lack of SFR–density relation amongst SF galaxies (Balogh et al. 2004; Wijesinghe et al. 2012), but our result sugggests that there is small, but significant environmental dependence of $SSFR$ for SF galaxies. Because the scatter of the SF main sequence is reported to be small (~0.3-dex; e.g. Elbaz et al. 2007), the ~0.1-dex environmental dependence of $SSFR$ would not be negligible. We need to consider this effect when we discuss environmental dependence of $T_{\rm dust}$ (see Section 4.3).

We comment that the $SSFR_{\rm IR}$ tends to be slightly higher than the $SSFR_{\rm SDSS}$ (~0.05-dex level) as can be seen in Fig. 9. Actually, this small offset can also be seen in Fig. 8. The reason is unclear, but this small difference between $SFR_{\rm SDSS}$ and $SFR_{\rm IR}$ has no significant effect on our main conclusion at all.

Our results are consistent with several recent studies

which reported the decline in $SSFR$ of SF galaxies in high-density environments. For example, Haines et al. (2013) found that the $SSFR$ of SF galaxies in clusters is systematically (∼ 28%) lower than their counterparts in the field, which is qualitatively consistent with our results. Fuller et al. (2016) also found that $SSFR$s of late type galaxies in the Coma cluster decrease monotonically with increasing local galaxy number density by using the *Herschel* Astrophysical Terahertz Large Area Survey (H-ATLAS) data. The environmental difference in $SSFR$ reported by Fuller et al. (2016) is ∼ 1-dex level at maximum, which is much larger than our result. Although the exact reason of this difference is not clear, a potential reason would be the different environmental range considered in their studies and our current work. We also note that their late-type galaxy sample is morphologically selected, while our star-forming galaxy sample is selected with the emission line properties.

4 DUST TEMPERATURE VERSUS ENVIRONMENT

4.1 Derivation of $T_{\rm dust}$

We derive $T_{\rm dust}$ using the FIR multi-band photometry obtained by our stacking analysis (see Section 2.2.2). In order to estimate the average $T_{\rm dust}$ for each subsample of SDSS SF galaxies, we here assume a single modified blackbody function:

$$\begin{aligned} F_\nu &= C\nu^\beta B_\nu(T_{\rm dust}) \\ &= C\frac{\nu^{3+\beta}}{\exp(h\nu/kT_{\rm dust})-1} \\ &= C\frac{(c/\lambda)^{3+\beta}}{\exp[(hc/\lambda)/kT_{\rm dust}]-1}, \end{aligned} \tag{13}$$

where F_ν is the flux density, β is the dust emissivity spectral index, C is a free-floating normalization factor, and B_ν is the Planck blackbody radiation function. Following many other works studying dust temperature in galaxies, we fix $\beta = 1.5$ in this study.

As discussed in Sec 2.2, we calculate the dust temperature using the flux densities at 90 and 140 μm, which straddle the peak of FIR SEDs of SF galaxies. Using equation (13), the ratio of the flux densities in the two bands can be written as:

$$\frac{F_{\nu_2}}{F_{\nu_1}} = \frac{\nu_2^{3+\beta}[\exp(h\nu_1/kT_{\rm dust})-1]}{\nu_1^{3+\beta}[\exp(h\nu_2/kT_{\rm dust})-1]}, \tag{14}$$

where F_{ν_1} and F_{ν_2} are the flux densities at 90 and 140 μm, respectively. This equation can then be approximated as:

$$\ln\frac{F_{\nu_2}}{F_{\nu_1}} \approx (3+\beta)\ln\frac{\nu_2}{\nu_1} + \frac{h}{kT}(\nu_1-\nu_2). \tag{15}$$

We checked that the difference between the F_{ν_2}/F_{ν_1} value from the equation (14) and (15) for $\beta = 1.5$ and $10 < T_{\rm dust} < 30$ is only 2% at maximum, which does not affect our results. Therefore, we can analytically derive $T_{\rm dust}$ with the following equation:

$$\begin{aligned} T_{\rm dust} &\approx \frac{h(\nu_1-\nu_2)/k}{\ln\frac{F_{\nu_2}}{F_{\nu_1}} - (3+\beta)\ln\frac{\nu_2}{\nu_1}} \\ &= \frac{\frac{hc}{k}(\frac{1}{\lambda_1}-\frac{1}{\lambda_2})}{\ln\frac{F_{\nu_2}}{F_{\nu_1}} - (3+\beta)\ln\frac{\lambda_1}{\lambda_2}}. \end{aligned} \tag{16}$$

We believe that this analytical approach is advantageous in the sense that it is always reproducible. One thing we should note is that the assumption of β value can affect the measurement of $T_{\rm dust}$: e.g. if we assume $\beta = 2.0$, the resultant $T_{\rm dust}$ becomes lower (typically by ∼ 2 K) than those derived under the assumption of $\beta = 1.5$. Therefore the *absolute* values of $T_{\rm dust}$ should be interpreted with care, but we stress that our *internal* comparisons (i.e. stellar mass, SFR, or environmental dependence of $T_{\rm dust}$) shown in this paper would not be affected by this uncertainty.

Following many other works studying dust temperature in galaxies, we assume the constant β value when studying the environmental effects on $T_{\rm dust}$.

4.2 $T_{\rm dust}$ as a function of galaxy properties

Before investigating the environmental effects on $T_{\rm dust}$, we examine the dependence of $T_{\rm dust}$ on various galaxy properties (e.g. M_*, SFR, and $SSFR$). We here divide the full SDSS SF galaxy sample into ten $M_*/SFR_{\rm SDSS}/SSFR_{\rm SDSS}$ bins, and perform FIR stacking analysis for each subsample.

In the left and middle panel of Fig. 10, we plot $T_{\rm dust}$ as a function of M_* and SFR, respectively. It can be seen that $T_{\rm dust}$ increases with SFR, while $T_{\rm dust}$ decreases with increasing M_*. We note that we use SDSS-based $SFR/SSFR$ to split the sample, but the plotted date points show IR-based measurements from stacking analyses. We note that the $T_{\rm dust}$–SFR correlation reported here is equivalent to the $T_{\rm dust}$–$L_{\rm IR}$ correlation shown by many recent studies (e.g. Totani & Takeuchi 2002; Blain et al. 2003; Hwang et al. 2010).

In the right panel of Fig. 10, we plot $T_{\rm dust}$ against $SSFR_{\rm IR}$; we here divide the sample into ten $SSFR_{\rm SDSS}$ bins and perform stacking analysis in the same way as above. The dashed line shows the result from best line fit. The increasing trend of $T_{\rm dust}$ with $SSFR$ is consistent with the results shown by Magnelli et al. (2014), although our derived $T_{\rm dust}$ values tend to be slightly lower than those of Magnelli et al. (2014) by ∼1–2 K. We here note again that most of our discussions presented in this paper are based on the *relative* comparison between our subsamples, and are not affected by the absolute value of $T_{\rm dust}$.

It is clear that there is a strong positive correlation between dust temperature and $SSFR_{\rm IR}$. Because $SSFR$ reflects the strength of UV radiation fields due to young massive stars in galaxies and the UV radiation heats up the dust content, it is expected that galaxies with higher $SSFR$ tend to have warmer dust temperatures, whereas galaxies with lower $SSFR$ should have colder dust temperatures (Magnelli et al. 2014).

Fig. 10 suggests that $T_{\rm dust}$ is most strongly correlated with $SSFR$, compared with M_* or SFR. This is not surprising because the $T_{\rm dust}$–$SSFR$ relation reflects the negative correlation between $T_{\rm dust}$ and M_*, as well as the positive correlation between $T_{\rm dust}$ and SFR. We need to consider this strong dependence of $T_{\rm dust}$ on $SSFR$ when we discuss environmental dependence of $T_{\rm dust}$.

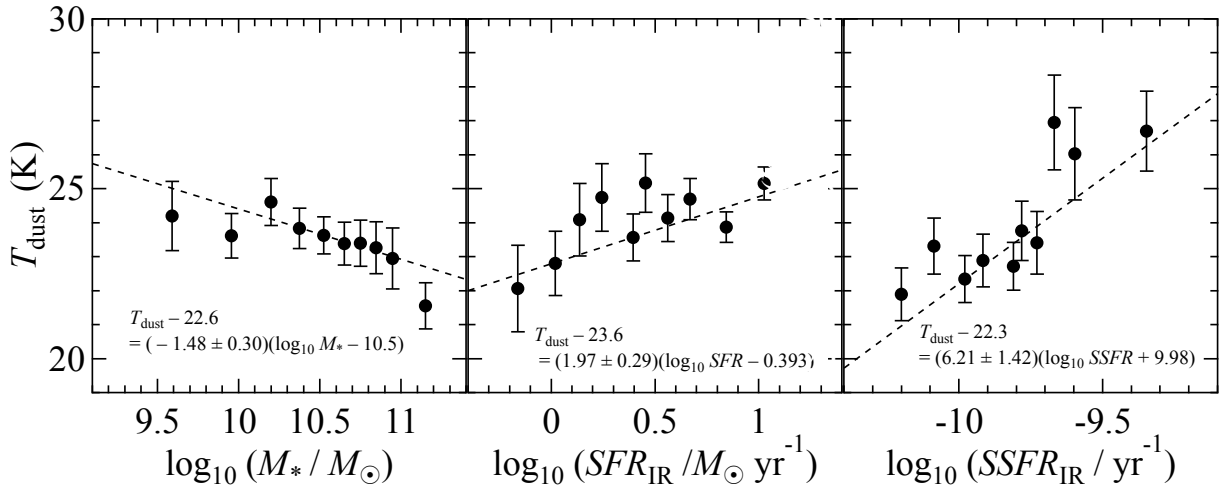

Figure 10. Average $T_{\rm dust}$ of SF galaxies as a function of M_* (left), SFR (middle), and $SSFR$ (right). In each panel, we split the sample into ten subsamples and perform FIR stacking analysis, to investigate the trend of $T_{\rm dust}$ with these physical properties of galaxies. The dashed line indicates the line fitting result in the case we adopt a pivot point of $\log_{10} M_* = 10.5$, $\log_{10} SFR = 0.393$ and $\log_{10} SSFR = -9.98$. Note that the results do not change much even if we performed the line fits without any pivot points.

4.3 Environmental dependence of $T_{\rm dust}$

This section presents the main results of this paper: i.e. the environmental dependence of $T_{\rm dust}$. We note that the combination of the wide-field coverage of SDSS and its entire coverage by the AKARI all-sky survey map allows us to perform the first systematic study of dust temperature of SF galaxies as a function of environment.

We recall that we defined the five environment bins (D1–D5) based on the local density of galaxies (see Section 2.1.1). As a first step, we show in Fig. 11(a) the $T_{\rm dust}$ derived for the D1–D5 samples. It would be interesting to note that $T_{\rm dust}$ mildly *increases* with increasing environmental density. The best fit line in the panel (a) derived with all the star-forming galaxies corresponds to:

$$T_{\rm dust}({\rm K}) = (23.8 \pm 0.3) + (0.90 \pm 0.71) \times \log_{10} \rho_5. \quad (17)$$

It turns out that the slope of this line is significantly positive (at 1.5σ level) with the probability of ~80%. In Section 3.2, we reported that $SSFR$ of SF galaxies *decrease* with increasing local density. On the other hand, we also found that there is an *increasing* trend of $T_{\rm dust}$ with $SSFR$ (see Section 4.2). By combining these two results, it is expected that $T_{\rm dust}$ should *decreases* with density—but the data suggests an opposite trend. We admit that the increasing trend is mostly driven by the data points of the lowest-density bin (D1), but we verify that our results are unchanged even when we split the sample into 10 environmental bins (although the errorbars of individual data points become larger in this case).

To investigate this trend more in detail, we further divide the D1–D5 sample into three $SSFR_{\rm SDSS}$ bins and perform the same stacking analyses to derive $T_{\rm dust}$. The results are shown in the panels (b)–(d) of Fig. 11. The error bars are clearly larger because of the smaller sample size, in particular for the panel-(d) because galaxies with higher $SSFR_{\rm SDSS}$ tend to have lower stellar mass or lower luminosity. Although the statistics is poor, it is notable that the same increasing trend of $T_{\rm dust}$–ρ_5 relation can be seen in all the cases.

We also examine the dependence of the $T_{\rm dust}$–$SSFR_{\rm IR}$ relation on ρ_5. In each panel of Fig. 12, we plot $T_{\rm dust}$ against $SSFR_{\rm IR}$ at fixed environment and compare them with the best-fit $T_{\rm dust}$–$SSFR_{\rm IR}$ relation derived for all SF galaxies (i.e. dashed line in the right panel of Fig. 10). Fig. 12 is equivalent to the panel (b)–(d) of Fig. 11, but we can now confirm that the $T_{\rm dust}$–$SSFR$ correlation is in place in all the environments. In other words, we need to remove the influence of $SSFR$ to discuss the environmental dependence of $T_{\rm dust}$ more robustly. For this purpose, we here define the offset value ($\Delta T_{\rm dust}$) of the data points from the best-fitted $T_{\rm dust}$–$SSFR_{\rm IR}$ line (see Fig. 12) as follows:

$$\Delta T_{\rm dust} = T_{\rm dust} - T_{\rm dust,exp}, \quad (18)$$

where $T_{\rm dust,exp}$ is the expected $T_{\rm dust}$ estimated from the best fitted $T_{\rm dust}$–$SSFR$ relation. In Fig. 13, we show $\Delta T_{\rm dust}$ for each environment. The dashed lines in this plot show the best-fit lines. The best fit line in the panel (a) derived with all the galaxies corresponds to:

$$\Delta T_{\rm dust}({\rm K}) = (0.41 \pm 0.33) + (1.24 \pm 0.77) \times \log_{10} \rho_5. \quad (19)$$

It should be noted that there still remains a positive correlation between $\Delta T_{\rm dust}$ and ρ_5. Interestingly, we find similar trends even when we further divide D1–D5 sample into three $SSFR_{\rm SDSS}$ bins (see Fig. 13 (b)–(d)). Our results suggest that $T_{\rm dust}$ increases with ρ_5 from low to high-density environment at fixed $SSFR$, and therefore the environmental effects on $T_{\rm dust}$ of SF galaxies should work over wide environmental range, and are not necessarily cluster-specific mechanisms. We note, however, that the average environmental difference reported here is only ~3 K at maximum over the ~2-dex local density range (D1–D5). Therefore, our conclusion is that the environmental impacts on dust temperature in SF galaxies

are much milder than that of $SSFR$, but we suggest that the environment should have some impacts on dust temperature in SF galaxies.

4.4 Discussion

Dust temperature in galaxies is expected to provide us with an important information on the geometry of star formation taking place inside the galaxies (e.g. Elbaz et al. 2011). In this paper, we reported a marginal trend that $T_{\rm dust}$ (as well as $\Delta T_{\rm dust}$) increases with environmental density (ρ_5).

The environmental impacts on dust properties of galaxies have not yet been studied well, but a few recent studies argue possible relationship between dust temperature and environment. Rawle et al. (2012) found that some galaxies (with $\log_{10}(L_{\rm IR}/L_\odot) < 11$) in the Bullet Cluster at $z \sim 0.3$ have *warmer* dust temperature (by ~7 K) than field galaxies with same luminosity using *Herschel* data. They suggested that dust stripping is the responsible mechanism for the unusually warm dust temperature, as the stripping effect can more easily strip cold dust from outskirts of galaxies. However, it is also true that ~ 90% of their star-forming cluster galaxies have dust temperatures similar to field galaxies with comparable $L_{\rm IR}$. We expect that the moderate rise of $T_{\rm dust}$ in higher-density environments reported by our analyses is qualitatively consistent with the results shown by Rawle et al. (2012).

Another supporting evidence has also been brought by some recent studies on the environmental dependence of dust *extinction* levels of galaxies. Koyama et al. (2013) found a positive correlation (~ 0.5 mag level) between dust extinction ($A_{\rm H\alpha}$) and local density for $z = 0.4$ SF galaxies, by comparing the IR- and Hα-based SFRs. They attributed the result to galaxy–galaxy interactions/mergers or gas/dust stripping resulting in a more compact configuration of star formation for SF galaxies residing in high-density environments. This environmental dependence of dust extinction levels of SF galaxies has recently been confirmed with Balmer decrement analysis with optical spectroscopy (Sobral et al. 2016). We believe that these results may also be linked to the increment of $T_{\rm dust}$ with local density suggested by our current work.

However, the environmental impacts on dust properties of galaxies are still controversial. Noble et al. (2015) performed FIR studies of $z \sim 1.2$ clusters, and showed that the dust temperature does not strongly correlate with environment, except for a $\sim 4\sigma$ drop in the average $T_{\rm dust}$ in an intermediate-density environment. They interpreted this result as invoking ram-pressure stripping of the warmer dust and reheating of the cold dust by the radiation of new stars which are formed by the surviving molecular gas. However, we cannot confirm such a sharp decline of $T_{\rm dust}$ at any environment bin at least for our $z = 0$ SF galaxies sample. Fuller et al. (2016) showed that the dust temperatures of late-type galaxies in the Coma cluster are hotter than those in the filamentary structure around the cluster, but the difference is small ($\lesssim 1$ K) and has no statistical significance. We should note, however, that our highest local density region (D5) covers relatively wide environmental range from clusters to surrounding filaments (see Fig. 4), and so a direct comparison between our results and those derived from studies on individual clusters would not be possible.

Regarding the environmental effects on dust extinction, Patel et al. (2011) showed that the dust extinction (A_V) for SF galaxies from SED fitting declines by ~ 0.5 mag from low to high local density at $0.6 < z < 0.9$. On the other hand, Garn et al. (2010) showed that $A_{\rm H\alpha}$ has no significant dependence on environment for Hα-selected galaxies at $z = 0.84$. In these ways, environmental effects on dust properties of galaxies are still under debate. More studies are clearly needed to understand the environmental effects on dust properties of galaxies.

We finally comment that it is not possible to determine β value with our current dataset. There is no study which explicitly reported environmental dependence (or independence) of β, and actually it is very hard to determine $T_{\rm dust}$ and β separately because $T_{\rm dust}$ and β are degenerate. As we briefly discussed in Section 4.1, the estimated $T_{\rm dust}$ can be slightly increased by assuming smaller β value. Therefore the marginal trend between $T_{\rm dust}$ and ρ_5 could be invoked by a reduction of β with increasing ρ_5. More detailed studies on β are needed to determine the cause of the relation between $T_{\rm dust}$ and ρ_5.

5 SUMMARY

In this paper, we present infrared views of the environmental effects on dust properties in star-forming (SF) galaxies at $z \sim 0$. In order to reveal the effects statistically, we use the AKARI FIS all-sky map and the large spectroscopic galaxy sample from SDSS DR7. We define the normalized local galaxy density (ρ_5) for each galaxy, which represents the ratio of its fifth nearest neighbour surface density to the mean density for all galaxies within a redshift slice of $\Delta z = \pm 0.003$ in SDSS. In this study, we use galaxies within the redshift range of $0.05 < z < 0.07$ and the stellar mass range of $9.2 < \log_{10}(M_*/M_\odot)$. We select SF galaxies based on their Hα equivalent widths ($EW_{\rm H\alpha} > 4$ Å) and emission line flux ratios using the BPT diagram. We then split them into five local density bins: D1–D5.

In order to investigate average FIR properties of SF galaxies, we perform FIR stacking analyses by splitting the SDSS SF galaxy sample according to their stellar mass, (S)SFR, and environment. We derive total infrared luminosity ($L_{\rm IR}$) for each subsample using the average flux densities at WIDE-S (90 μm) and WIDE-L (140 μm) bands, and then compute IR-based SFR ($SFR_{\rm IR}$) from $L_{\rm IR}$. We find that $SSFR_{\rm IR}$ of SF galaxies decreases monotonically from the low to high density regions. We note that the environmental difference is not large (~ 0.1 dex level even if we compare the lowest- and highest-density bins), but this decline in star formation activity *amongst SF galaxies* suggests that the environmental effects do not simply shut down the SF activity instantly, implying a slow quenching mechanism (e.g. strangulation) at work over wide environmental range.

We also derive average dust temperature ($T_{\rm dust}$) of SF galaxies using the flux densities at 90 μm and 140 μm bands. We study the dependence of $T_{\rm dust}$ on galaxy properties, and confirm a strong positive correlation between $T_{\rm dust}$ and $SSFR_{\rm IR}$, consistent with recent studies. We investigate the environmental impacts on the average $T_{\rm dust}$ of SF galaxies, and find an interesting hint that $T_{\rm dust}$ increases with increasing environmental density. Although the environmental

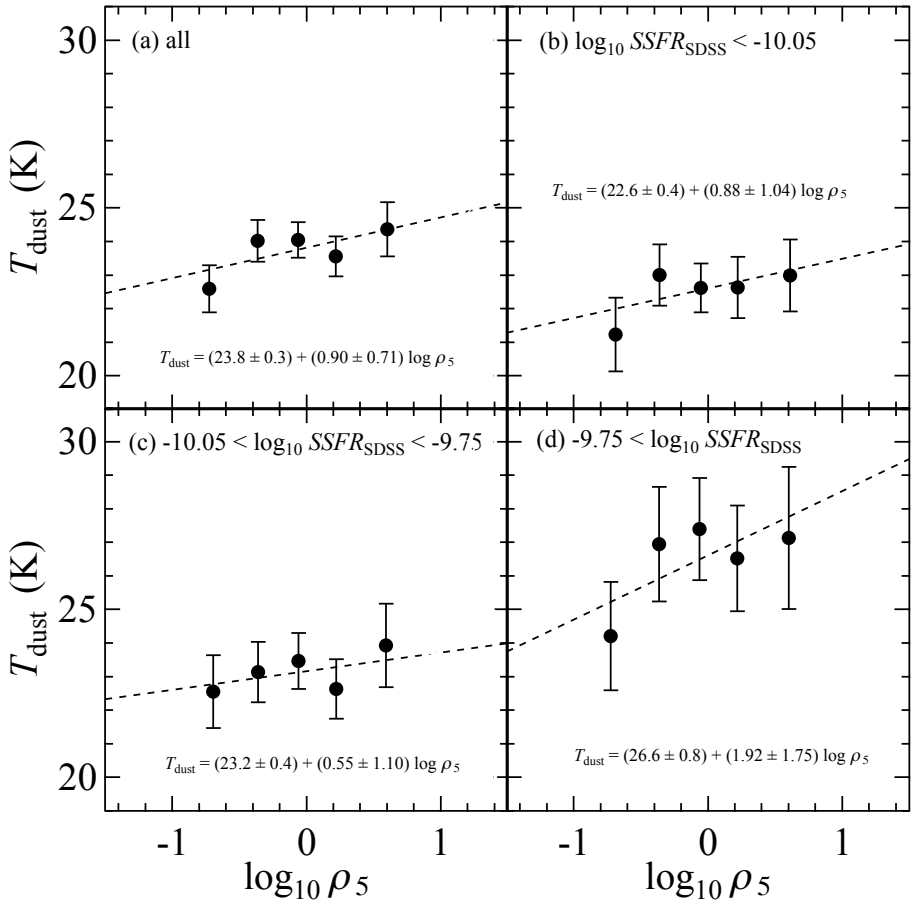
(a) all
(b) log10 SSFRSDSS < -10.05
(c) -10.05 < log10 SSFRSDSS < -9.75
(d) -9.75 < log10 SSFRSDSS
Tdust = (23.8 ± 0.3) + (0.90 ± 0.71) log ρ5
Tdust = (22.6 ± 0.4) + (0.88 ± 1.04) log ρ5
Tdust = (23.2 ± 0.4) + (0.55 ± 1.10) log ρ5
Tdust = (26.6 ± 0.8) + (1.92 ± 1.75) log ρ5
Tdust (K)
log10 ρ5

Figure 11. (a): Dependence of $T_{\rm dust}$ on the local galaxy density (ρ_5) for all the sample. (b)–(d): The same plot for three $SSFR_{\rm SDSS}$ bins. In all these panels, $T_{\rm dust}$ are derived from the 90 and 140 μm data (with equation (16)). The definition of the $SSFR_{\rm SDSS}$ range is indicated in each panel. The dashed lines correspond to the best-fit line.

trend is much milder (and only marginal) than the $SSFR$–$T_{\rm dust}$ correlation, our results suggest that the environmental effects may affect dust temperature in SF galaxies. The physical mechanism which is responsible for this phenomenon is not clear, but we suggest that it is not necessarily a cluster-specific mechanism because $T_{\rm dust}$ monotonically increases from lowest- to highest-density environments. We note that our results do not change even if we consider the small environmental difference in $SSFR$; i.e we confirm that the offset value from the $SSFR$–$T_{\rm dust}$ relation ($\Delta T_{\rm dust}$) shows the same environmental trend as that for $T_{\rm dust}$.

This paper provides the first systematic study on the environmental dependence of the dust temperature in SF galaxies by taking advantage of the wide-field (all-sky) coverage at FIR with the newly released AKARI FIS map. We find a marginal, but potentially an important hint that the average $T_{\rm dust}$ of SF galaxies may increase with environmental density. We note that the weak environmental trend could also be caused by a reduction of β with increasing ρ_5, but in any case, our study suggests that dust properties in SF galaxies (dust temperature and/or dust composition) may depend on environment. More detailed studies on individual galaxies, particularly spatially resolved studies of dust properties within the galaxies (with high-resolution FIR–submm observations), are needed to identify physical properties that produce the environmental trend we reported in this paper.

ACKNOWLEDGMENTS

We thank the referee for reviewing our paper and giving us valuable advice which improved the paper. This research is based on observations with AKARI, a JAXA project with the participation of ESA. We thank Prof. Kotaro Kohno and Prof. Hideo Matsuhara for their valuable advice to our study. This work was financially supported in part by a Grant-in-Aid for the Scientific Research (No. 25247016, 26247030, 26800107) by the Japanese Ministry of Education, Culture, Sports and Science.

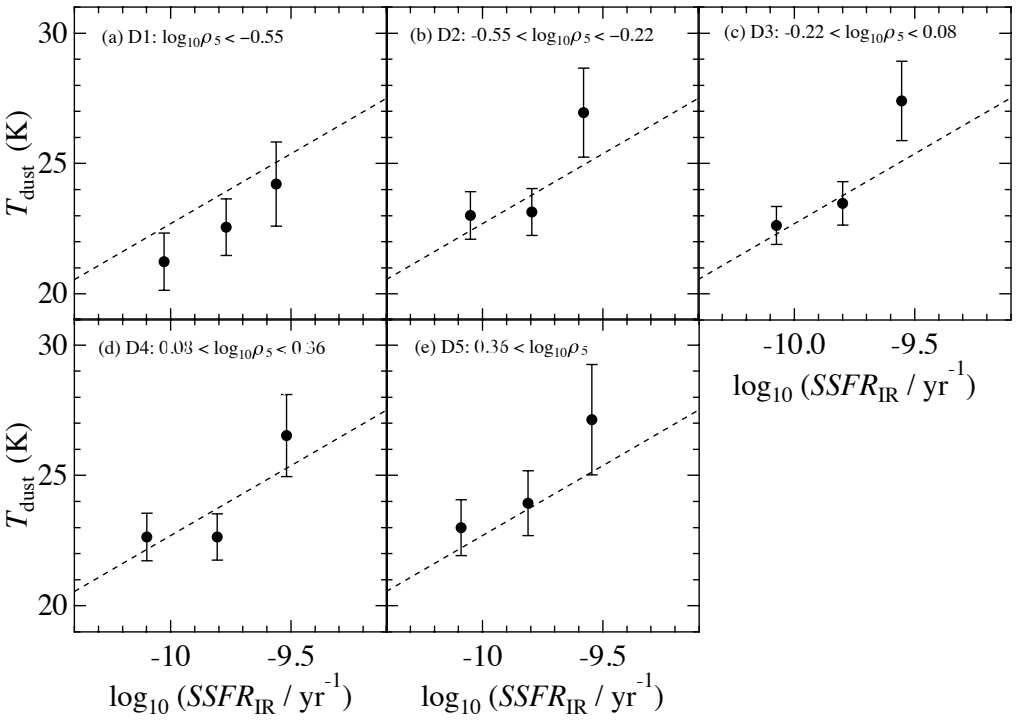

Figure 12. Dependence of $T_{\rm dust}$ on $SSFR_{\rm IR}$ at fixed local galaxy number density (D1–D5 sample). The dashed line in each panel corresponds to the best-fit line in the right panel of Fig. 10. The clear $T_{\rm dust}$–$SSFR$ correlation can be seen in all environments.

REFERENCES

Abazajian K. N., et al., 2009, ApJS, 182, 543
Arimatsu K., Doi Y., Wada T., Takita S., Kawada M., Matsuura S., Ootsubo T., Kataza H., 2014, PASJ, 66, 47
Baldwin J. A., Phillips M. M., Terlevich R., 1981, PASP, 93, 5
Balogh M. L., Morris S. L., Yee H. K. C., Carlberg R. G., Ellingson E., 1997, ApJ, 488, L75
Balogh M., et al., 2004, MNRAS, 348, 1355
Bekki K., 2009, MNRAS, 399, 2221
Blain A. W., Barnard V. E., Chapman S. C., 2003, MNRAS, 338, 733
Blanton M. R., Moustakas J., 2009, ARA&A, 47, 159
Brinchmann J., Charlot S., White S. D. M., Tremonti C., Kauffmann G., Heckman T., Brinkmann J., 2004, MNRAS, 351, 1151
Charlot S., Longhetti M., 2001, MNRAS, 323, 887
Chary R., Elbaz D., 2001, ApJ, 556, 562
Compiègne M., Flagey N., Noriega-Crespo A., Martin P. G., Bernard J.-P., Paladini R., Molinari S., 2010, ApJ, 724, L44
Cortese L., et al., 2012, A&A, 540, A52
Daddi E., et al., 2007, ApJ, 670, 156
Diemand J., Kuhlen M., Madau P., 2007, ApJ, 667, 859
Doi Y., et al., 2015, PASJ, 67, 50
Draine B. T., 2003, ARA&A, 41, 241
Dressler A., 1980, ApJ, 236, 351
Elbaz D., et al., 2007, A&A, 468, 33
Elbaz D., et al., 2011, A&A, 533, A119
Engelbracht C. W., et al., 2010, A&A, 518, L56
Feldmann R., Carollo C. M., Mayer L., 2011, ApJ, 736, 88
Fuller C., et al., 2016, MNRAS,
Garn T., et al., 2010, MNRAS, 402, 2017
Gómez P. L., et al., 2003, ApJ, 584, 210
Goto T., Yamauchi C., Fujita Y., Okamura S., Sekiguchi M., Smail I., Bernardi M., Gomez P. L., 2003, MNRAS, 346, 601
Gunn J. E., Gott III J. R., 1972, ApJ, 176, 1
Haines C. P., et al., 2013, ApJ, 775, 126
Hirashita H., Kaneda H., Onaka T., Suzuki T., 2008, PASJ, 60, 477
Hwang H. S., et al., 2010, MNRAS, 409, 75
Kauffmann G., et al., 2003a, MNRAS, 341, 33
Kauffmann G., et al., 2003b, MNRAS, 346, 1055
Kawada M., et al., 2007, PASJ, 59, S389
Kawata D., Mulchaey J. S., 2008, ApJ, 672, L103
Kennicutt Jr. R. C., 1998, ARA&A, 36, 189
Kewley L. J., Heisler C. A., Dopita M. A., Lumsden S., 2001, ApJS, 132, 37
Kewley L. J., Jansen R. A., Geller M. J., 2005, PASP, 117, 227
Koyama Y., Kodama T., Shimasaku K., Hayashi M., Okamura S., Tanaka I., Tokoku C., 2010, MNRAS, 403, 1611
Koyama Y., et al., 2013, MNRAS, 434, 423
Koyama Y., et al., 2015, MNRAS, 453, 879
Kroupa P., 2001, MNRAS, 322, 231
Larson R. B., Tinsley B. M., Caldwell C. N., 1980, ApJ, 237, 692
Lewis I., et al., 2002, MNRAS, 334, 673
Magnelli B., et al., 2014, A&A, 561, A86
Moore B., Lake G., Quinn T., Stadel J., 1999, MNRAS, 304, 465
Murakami H., et al., 2007, PASJ, 59, 369
Noble A. G., Webb T. M. A., Yee H. K. C., Muzzin A., Wilson G., van der Burg R. F. J., Balogh M. L., Shupe D. L., 2015, preprint, (arXiv:1511.00584)
Noeske K. G., et al., 2007, ApJ, 660, L43
Patel S. G., Kelson D. D., Holden B. P., Franx M., Illingworth G. D., 2011, ApJ, 735, 53
Peng Y.-j., et al., 2010, ApJ, 721, 193

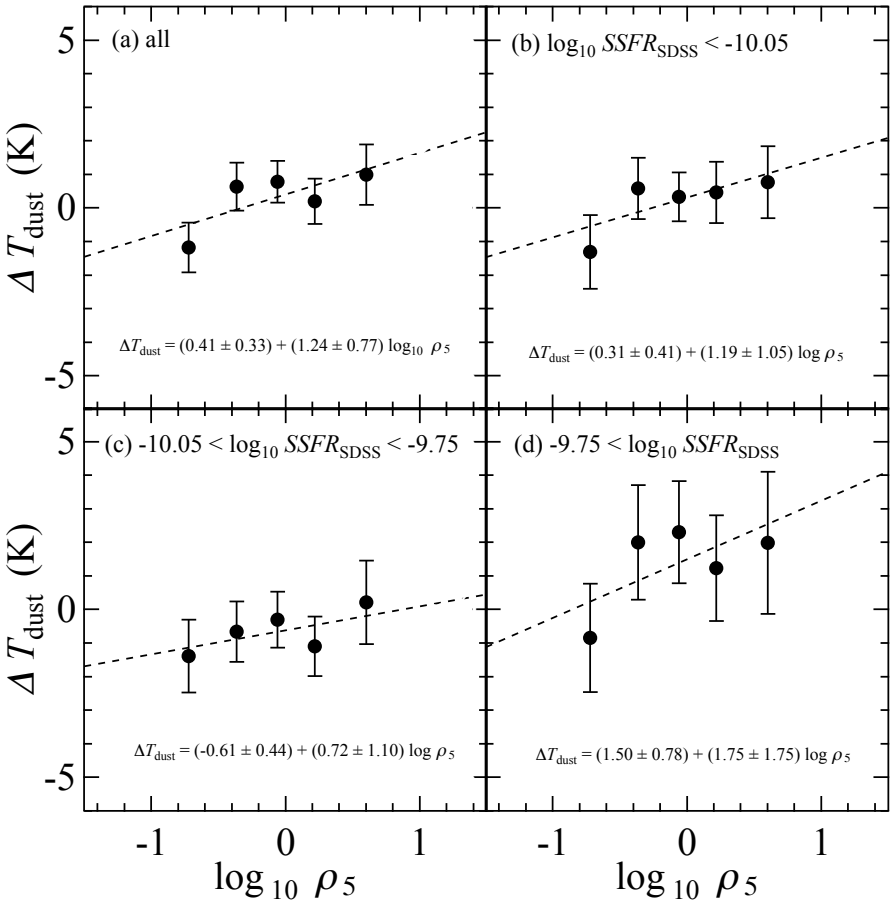
(a) all
(b) log10 SSFRSDSS < -10.05
(c) -10.05 < log10 SSFRSDSS < -9.75
(d) -9.75 < log10 SSFRSDSS
ΔTdust = (0.41 ± 0.33) + (1.24 ± 0.77) log10 ρ5
ΔTdust = (0.31 ± 0.41) + (1.19 ± 1.05) log ρ5
ΔTdust = (-0.61 ± 0.44) + (0.72 ± 1.10) log ρ5
ΔTdust = (1.50 ± 0.78) + (1.75 ± 1.75) log ρ5
Δ Tdust (K)
log 10 ρ5
5
0
-5
-1
1

Figure 13. (a): Environmental dependence of the average offset values ($\Delta T_{\rm dust}$) from the best fit $T_{\rm dust}$–$SSFR_{\rm IR}$ derived with all star-forming galaxies (Fig. 10). (b)–(d): the same plot in each $SSFR_{\rm SDSS}$ bin. The dashed lines correspond to the best line fits.

Petrosian V., 1976, ApJ, 209, L1

Poggianti B. M., Wu H., 2000, ApJ, 529, 157

Quilis V., Moore B., Bower R., 2000, Science, 288, 1617

Rawle T. D., et al., 2012, ApJ, 756, 106

Salim S., et al., 2007, ApJS, 173, 267

Sobral D., Stroe A., Koyama Y., Darvish B., Calhau J. a., Afonso A., Kodama T., Nakata F., 2016, MNRAS,

Takeuchi T. T., Buat V., Heinis S., Giovannoli E., Yuan F.-T., Iglesias-Páramo J., Murata K. L., Burgarella D., 2010, A&A, 514, A4

Takita S., et al., 2015, PASJ, 67, 51

Totani T., Takeuchi T. T., 2002, ApJ, 570, 470

Vulcani B., Poggianti B. M., Finn R. A., Rudnick G., Desai V., Bamford S., 2010, ApJ, 710, L1

Whitaker K. E., van Dokkum P. G., Brammer G., Franx M., 2012, ApJ, 754, L29

Wijesinghe D. B., et al., 2012, MNRAS, 423, 3679

Yamamura I., et al., 2009, in Onaka T., White G. J., Nakagawa T., Yamamura I., eds, Astronomical Society of the Pacific Conference Series Vol. 418, AKARI, a Light to Illuminate the Misty Universe. p. 3

Zabludoff A. I., Mulchaey J. S., 1998, ApJ, 496, 39

This paper has been typeset from a TEX/LATEX file prepared by the author.